Available online at www.sciencedirect.com
ScienceDirect
Trans. Nonferrous Met. Soc. China 35(2025) 1987−1995
Transactions of Nonferrous Metals Society of China
www.tnmsc.cn

# Construction and electrochemical performance of $NaCrO_2$@$Cr_2O_3$ cathode material for sodium-ion batteries

Mu-lan QIN[1#], Chao HU[2#], Guo-zhao FANG[2], Shu-quan LIANG[2], Wan-min LIU[1], Bin SHEN[1]

1. College of Materials and Chemical Engineering, Hunan Institute of Engineering, Xiangtan 411104, China;
2. School of Materials Science and Engineering, Central South University, Changsha 410083, China

Received 2 November 2024; accepted 29 April 2025

**Abstract:** The electrochemical performance of layered O3-type $NaCrO_2$ cathode material is significantly affected by the side reactions between $NaCrO_2$ and electrolyte during sodium storage. A uniform $Cr_2O_3$ coating layer was in situ constructed on the surface of $NaCrO_2$ by controlling the excess ratio of sodium source. The structure, morphology, valence and electrochemical performance of the $Cr_2O_3$-coated $NaCrO_2$ were characterized. The results indicate that the $Cr_2O_3$ coating layer does not alter the crystal structure and morphology of $NaCrO_2$, but effectively suppresses the side reactions between $NaCrO_2$ and electrolyte, and improves the surface/interfacial stability of $NaCrO_2$ material. The $Cr_2O_3$-coated $NaCrO_2$ exhibits improved electrochemical performance with a capacity retention of 66.4% after 500 cycles at 10*C*.

**Key words:** $NaCrO_2$; $Cr_2O_3$; sodium-ion battery; cathode material; electrochemical performance

## 1 Introduction

The rapid development of renewable energy, such as solar and wind energy, urgently requires low-cost energy storage systems. Although lithium-ion batteries (LIBs) have been widely adopted in portable devices and electric vehicles, the limited availability of lithium resources restricts their application in large-scale energy storage systems [1−3]. Sodium-ion batteries (SIBs) are considered to be one of the most promising alternatives to LIBs in the energy storage field, owing to their abundant sodium resources, favorable electrochemical performance, and environmental friendliness [4,5].

The development of suitable cathode materials is crucial for the commercialization of SIBs [5−7]. Layered transition metal oxides ($Na_xMO_2$, M= transition metal element, $0<x\leq1$) have attracted extensive research as cathode materials for SIBs due to their high electrochemical activity, superior capacity, and ease of synthesis [8−11]. In particular, layered O3-type $NaCrO_2$ stands out by virtue of certain remarkable advantages including a desirable flat charge/discharge voltages at around 3.0 V, high reversible capacity of 125 mA·h/g and excellent thermal stability [12−14]. However, $NaCrO_2$ experiences rapid capacity decay during cycling, primarily attributed to side reactions between the active material and the electrolyte, as well as structural instability caused by repeated $Na^+$ insertion/extraction [15−17].

To optimize the electrochemical performance of $NaCrO_2$, various modifications, such as carbon coating [18−20], heteroatom doping [21−25] and morphology control [26−28], have been reported. Carbon coating can enhance the electrical conductivity of the material to improve the electrochemical performance. YU et al [29] modified

# Mu-lan QIN and Chao HU contributed equally to this work
**Corresponding author:** Mu-lan QIN, Tel: +86-15773220865, E-mail: 70318@hnie.edu.cn
https://doi.org/10.1016/S1003-6326(25)66795-1

the surface of $NaCrO_2$ with carbon using pitch as the carbon source, and the electronic conductivity of the material increases to $10^{-1}$ S/cm. The carbon-coated $NaCrO_2$ exhibits an ultrafast rate capability up to 150*C* with a specific capacity of 99 mA·h/g. However, oxide coating, a common approach for modifying other electrode materials [30−32], has rarely been reported for $NaCrO_2$.

$Cr_2O_3$ produced as a by-product during the synthesis of $NaCrO_2$ is often regarded as an impurity phase because it reduces the specific capacity, although it has been used as a coating material in electrode materials for LIBs [33−35]. In recent years, the application of $Cr_2O_3$ in SIBs has also been reported, which can effectively increase the stability of the material's crystal structure and extend the cycle life of cathode at high current density. WANG et al [36] prepared in situ $Cr_2O_3$-coated $NaCrO_2$ with improved electrochemical performance by adding excess chromium. The capacity retention of $Cr_2O_3$-coated $NaCrO_2$ reaches 84.8% after 1000 cycles at 10*C*, and a specific capacity of 108 mA·h/g can still be obtained at a high rate of 60*C*. IKHE et al [37] reported $Cr_2O_3$-coated and Al-doped $NaCrO_2$ which shows excellent cyclic stability with no capacity decay during 1000 cycles at 5*C* with a capacity of 107 mA·h/g.

In this study, a uniform $Cr_2O_3$ coating layer was constructed on the surface of $NaCrO_2$ by controlling the excess ratio of sodium to chromium. The coating layer protects $NaCrO_2$ from severe side reactions and enhances the surface/interface stability during charge−discharge processes, thereby resulting in improved electrochemical performance of $NaCrO_2$ at high rates.

## 2 Experimental

### 2.1 Material synthesis

A facile sol−gel method was used to synthesize $NaCrO_2$ cathode material. In a typical process, $NaNO_3$ and $Cr(CH_3COO)_3$ were dissolved into $H_2O$ to obtain a clear solution. Citric acid used as a chelating agent was added into the solution, and then $NH_3·H_2O$ was added to adjust the pH value to 7. Subsequently, the solution was stirred and reacted at 70 °C for 5 h and then dried at 150 °C to form dry gel. Finally, the gel was annealed at 450 °C for 5 h in air and then calcined at 900 °C for 10 h under an $Ar/H_2$ atmosphere to obtain the sample. When the molar ratios of $NaNO_3$ and $Cr(CH_3COO)_3$ were set to 1.10∶1 and 1.05∶1, the synthesized samples were denoted as NCO-1.10 and NCO-1.05, respectively. In order to prevent the deterioration of material by the absorption of ambient moisture, the samples were stored in an Ar-filled glove box.

### 2.2 Material characterization

The crystallographic structures of samples were determined by X-ray power diffraction (XRD, Rigaku Mini Flex 600 with Cu $K_\alpha$ radiation, $\lambda$=1.5418 Å) over the $2\theta$ range of 10°−80°. The XRD patterns were refined via Rietveld program general structure analysis system (GSAS) software. The morphology and microstructure were characterized by field emission scanning electron microscopy (FESEM, FEI Nova NanoSEM 230) and transmission electron microscopy (TEM, FEI Titan G2 60−300) equipped with an X-ray energy dispersive spectrometer (EDS). The chemical valance state of each element on the surface was measured by X-ray photoelectron spectroscopy (XPS, VG Escalab−250xi).

### 2.3 Electrochemical evaluation

The electrochemical performances of the samples were tested in CR2025 cion cells. The working electrode was composed of active material, acetylene black and PVDF with a mass ratio of 8∶1∶1, and the loading of electrode was about 1.1 mg/cm$^2$. Sodium metal was used as the reference electrode and glass fiber (Whatman GF/D) was used as the separator. 1 mol/L $NaClO_4$ in ethylene carbonate (EC) + propylene carbonate (PC) (volume ratio of 1∶1) solution with 5 vol.% fluoroethylene carbonate (FEC) was used as the electrolyte. The galvanostatic charge/discharge measurements were performed on a Neware battery test system (CT−4008T−5V20mA−164). Cyclic voltammetry (CV) and electrochemical impedance spectroscopy (EIS, in the range from 100 kHz to 10 mHz) were conducted using an electrochemical workstation (CHI 660E).

## 3 Results and discussion

### 3.1 Physicochemical characteristics

During the sol−gel synthesis of $NaCrO_2$, $Na^+$ and $Cr^{3+}$ were mixed homogeneously in the gel, and in-situ $Cr_2O_3$-coated $NaCrO_2$, rather than

sodium-poor phase $Na_xCrO_2$ ($x$<1), was synthesized due to the volatilization of Na on the surface during calcination, although excess sodium was used. Figure 1 shows the XRD patterns of NCO-1.10 and NCO-1.05. As can be seen from Fig. 1(a), the main phase in the NCO-1.10 sample is the O3-type $NaCrO_2$ (JCPDS No. 25-0819). In sample NCO-1.05, in addition to the diffraction peaks belonging to $NaCrO_2$, new diffraction peaks located at 24.5°, 36.2°, 50.2° and 54.9° can be indexed to the $Cr_2O_3$ phase. The XRD patterns of NCO-1.10 and NCO-1.05 were further refined (Figs. 1(b, c)), and the lattice parameters are given in Table 1. The results show that when the excess content of sodium reaches 10%, the synthesized sample is $NaCrO_2$ pure phase with no heterogeneous phase. When the excess content of sodium decreases to 5%, a two-phase material consisting of 98.11 wt.% $NaCrO_2$ and 1.73 wt.% $Cr_2O_3$ is synthesized, denoted as $NaCrO_2$@$Cr_2O_3$. The structural parameters obtained by refinement are basically consistent with those reported in the literature [29,36]. There is almost no difference in the lattice parameters of the $NaCrO_2$ phase in the two samples, indicating that the $Cr_2O_3$ coating does not affect the crystal structure of $NaCrO_2$.

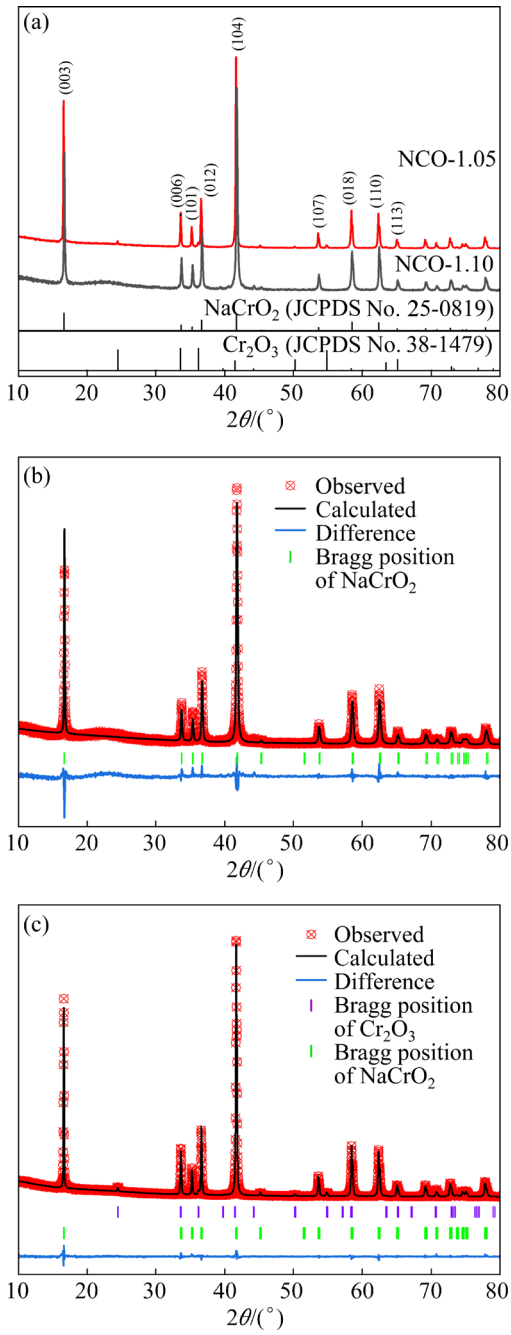


**Fig. 1** XRD patterns of NCO-1.10 and NCO-1.05 (a); Rietveld refinements of XRD patterns of NCO-1.10 (b) and NCO-1.05 (c)

**Table 1** XRD refinement results of NCO-1.10 and NCO-1.05

| Sample | $a$/Å | $c$/Å | $V$/Å$^3$ |
|---|---|---|---|
| NCO-1.10 | 2.9714 | 15.9573 | 122.015 |
| NCO-1.05−98.11%$NaCrO_2$ | 2.9737 | 15.9577 | 122.204 |
| NCO-1.05−1.73%$Cr_2O_3$ | 4.9581 | 13.5932 | 289.388 |

The morphology and microstructure of $NaCrO_2$ and $NaCrO_2$@$Cr_2O_3$ were characterized by SEM and TEM. As can be seen from Fig. 2, the samples, $NaCrO_2$ and $NaCrO_2$@$Cr_2O_3$, are composed of polygonal-shaped particles with particle size of about 1 μm, which suggests that the $Cr_2O_3$ coating has no influence on the powder morphology. In the HRTEM image of $NaCrO_2$@$Cr_2O_3$, a uniform coating layer with thickness of about 3 nm can be observed. The interplanar spacing of 0.373 nm observed on the particle edge (the inset in Fig. 2(d)) is in good agreement with the distance of neighboring (012) crystal planes of $Cr_2O_3$, which further confirms the presence of $Cr_2O_3$ coating layer. The EDS mapping images of $NaCrO_2$@$Cr_2O_3$ (Fig. 2(e)) show the homogeneous distribution of Na, Cr and O elements. The uniform $Cr_2O_3$ coating layer can prevent the direct contact between the $NaCrO_2$ and the electrolyte, and improve the surface/interfacial stability of $NaCrO_2$ material.

In order to explore the oxidation states of surface/interface elements in the $NaCrO_2$@$Cr_2O_3$, XPS analysis was further conducted. The XPS full spectrum (Fig. 3(a)) demonstrates the coexistence of Na, Cr and O elements in the $NaCrO_2$/$Cr_2O_3$.

The high-resolution Cr 2p spectrum and the corresponding fitted profiles are shown in Fig. 3(b). The Cr doublet in the Cr 2p spectrum is attributed to Cr $2p_{3/2}$ and Cr $2p_{1/2}$. The fitted peaks located at 578.13 and 588.63 eV are assigned to $Cr^{4+}$ $2p_{3/2}$ and $Cr^{4+}$ $2p_{1/2}$, respectively. In addition, the fitted peaks located at 575.83 and 585.58 eV are assigned to $Cr^{3+}$ $2p_{3/2}$ and $Cr^{3+}$ $2p_{1/2}$, respectively [24,38], which further proves that the coating layer on the surface of $NaCrO_2$ material is $Cr_2O_3$.

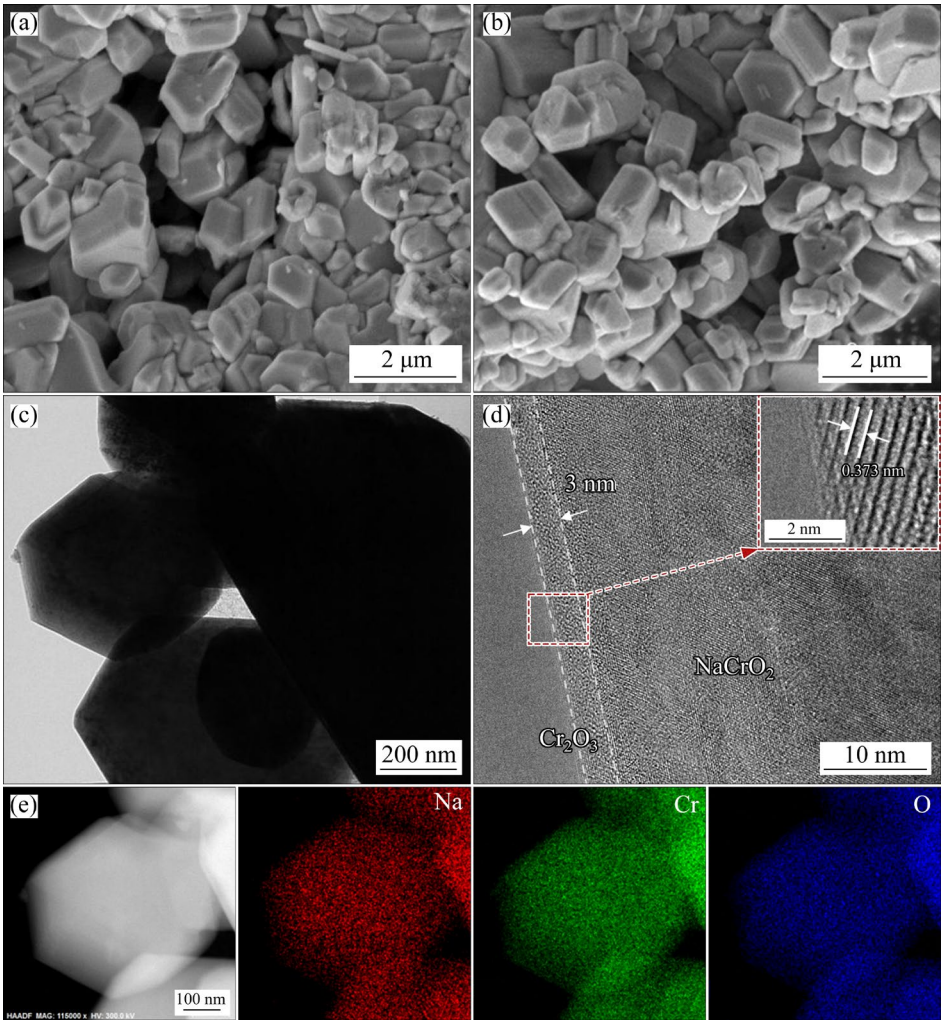


**Fig. 2** SEM images of $NaCrO_2$ (a) and $NaCrO_2@Cr_2O_3$ (b); TEM (c), HRTEM (d) and EDS mapping (e) images of $NaCrO_2@Cr_2O_3$

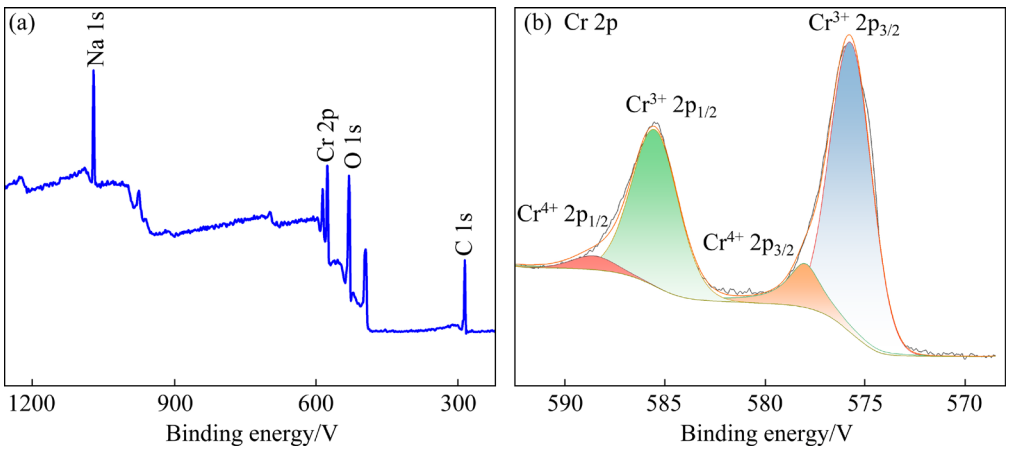


**Fig. 3** XPS full spectrum (a) and high-resolution Cr 2p spectrum (b) of $NaCrO_2@Cr_2O_3$

### 3.2 Electrochemical performance

The redox processes of the $NaCrO_2$ were first investigated by CV measurements. Figures 4(a) and 4(b) show initial three CV curves of $NaCrO_2$ and $NaCrO_2$@$Cr_2O_3$ between 2.0 and 3.6 V at a sweep rate of 0.1 mV/s, respectively. There are two apparent anodic peaks centered at 3.09 and 3.33 V, which correspond to the cathodic peaks at 2.92 and 3.28 V, respectively. These reversible peaks are assigned to the oxidation/reduction of $Cr^{3+}/Cr^{4+}$, suggesting the two major phase transitions (O3⇌O'3 ⇌ P'3) in the charge−discharge processes [36,39]. In addition, the other small peaks correspond to the order/disorder phase transformation [27,40]. The potential difference between the anodic and the cathodic peaks of $NaCrO_2$@$Cr_2O_3$ (0.17 V) is less than that of $NaCrO_2$ (0.21 V) after 3 cycles, indicating that the $NaCrO_2$@$Cr_2O_3$ sample has reduced polarization and improved electrochemical reversibility during cycling.

Figures 5(a) and 5(b) show the typical charge/discharge curves of $NaCrO_2$ and $NaCrO_2$@$Cr_2O_3$ at various *C*-rates (1*C*=125 mA·h/g) between 2.0 and 3.6 V, respectively. Two charge voltage plateaus located at 3.0 and 3.3 V along with their discharge counterparts at 2.9 and 3.3 V can be clearly observed in the charge/discharge curves at 1*C*, which are consistent with the CV curves shown in Fig. 4. The voltage platform at 2.8 V is likely due to the mismatch between the ester-based electrolyte and the anode, resulting in a sudden increase in polarization voltage during the later stages of sodium ion extraction from anode [41], which is also observed in the previous reports [26,42]. The polarization of the materials increases gradually with the increase of *C*-rate, and the polarization of $NaCrO_2$ is much greater than that of $NaCrO_2$@$Cr_2O_3$. Figure 5(c) shows the rate performance of $NaCrO_2$ and $NaCrO_2$@$Cr_2O_3$. The $NaCrO_2$ exhibits the specific capacities of 109.1, 101.4, 95.7, 85.4, and 58.4 mA·h/g at 1*C*, 2*C*, 3*C*, 5*C* and 10*C*, respectively. The decreased specific capacities of $NaCrO_2$@$Cr_2O_3$ at low rates are attributed to the inactive $Cr_2O_3$ coating layer with no capacity contribution. However, the $NaCrO_2$@$Cr_2O_3$ shows the specific capacities of 86.5 and 74.7 mA·h/g at 5*C* and 10*C*, respectively. The enhanced rate performance can be attributed to the uniform $Cr_2O_3$ coating layer on the surface of the $NaCrO_2$, which improves the surface/interfacial structure and effectively reduces the polarization of $NaCrO_2$, conducing to the rapid $Na^+$ insertion/extraction.

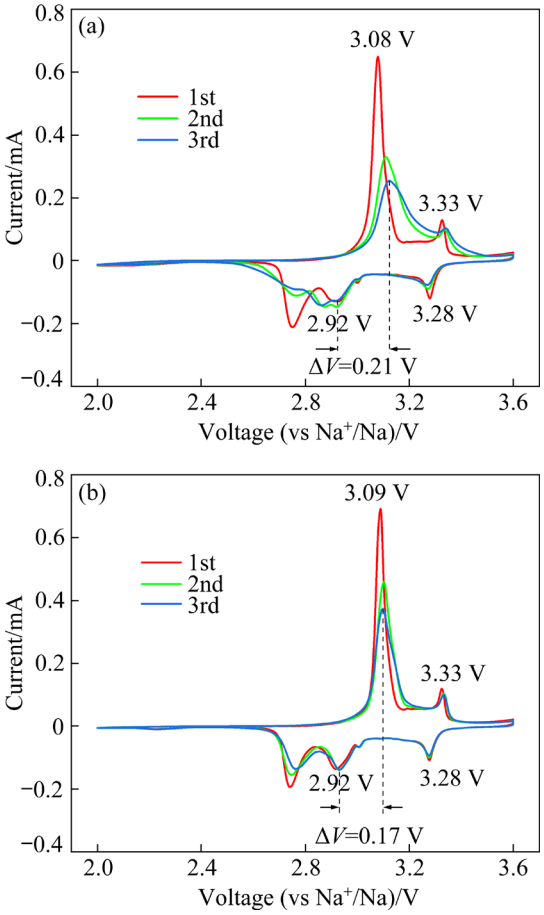


**Fig. 4** Initial three CV curves of $NaCrO_2$ (a) and $NaCrO_2$@$Cr_2O_3$ (b) at 0.1 mV/s

The cycling stability of samples at high rate is also explored, as shown in Fig. 5(d). After 500 cycles at 10*C*, the $NaCrO_2$@$Cr_2O_3$ shows a specific discharge capacity of 60.5 mA·h/g with a capacity retention of 66.4%, and the coulombic efficiency is close to 100% during cycling. However, the $NaCrO_2$ can only maintain 40.4 mA·h/g with a capacity retention of 40.3%. The enhanced cycling performance of $NaCrO_2$@$Cr_2O_3$ can be attributed to the uniform $Cr_2O_3$ coating layer which prevents the direct contact between the active material and the electrolyte, suppressing electrolyte decompositions and other side reactions effectively, and guaranteeing the electrode stability [36]. Compared with the literature [36−38], no significant electrochemical performance advantages of the synthesized material are observed. This may be attributed to several factors, including exposure to moist air during electrode preparation, mismatch between

the selected electrolyte and the electrode, and the thickness of the coating layer needed to be optimized. These factors require further investigation and verification.

In order to understand the effects of $Cr_2O_3$ coating on the cycling performance, d$Q$/d$V$ analyses of the discharge curves at the 10th, 30th and 50th cycles in Fig. 5(d) were performed. As shown in Fig. 6, two obvious reduction peaks centered at 2.80 and 3.13 V are observed in the d$Q$/d$V$ curve of $NaCrO_2$@$Cr_2O_3$ at the 10th cycle, corresponding to the reduction reaction of $Cr^{3+}/Cr^{4+}$. The higher reduction potential of $NaCrO_2$@$Cr_2O_3$ indicates higher energy. As the cycle number increases, the reduction peaks shift to lower potentials owing to the increased polarization. After 50 cycles, the difference value between the reduction potentials of $NaCrO_2$@$Cr_2O_3$ (0.05 V) is much less than that of $NaCrO_2$ (0.15 V). The reduced polarization of $NaCrO_2$@$Cr_2O_3$ can be attributed to the enhanced surface/interface stability, which is beneficial to improving the electrochemical performance.

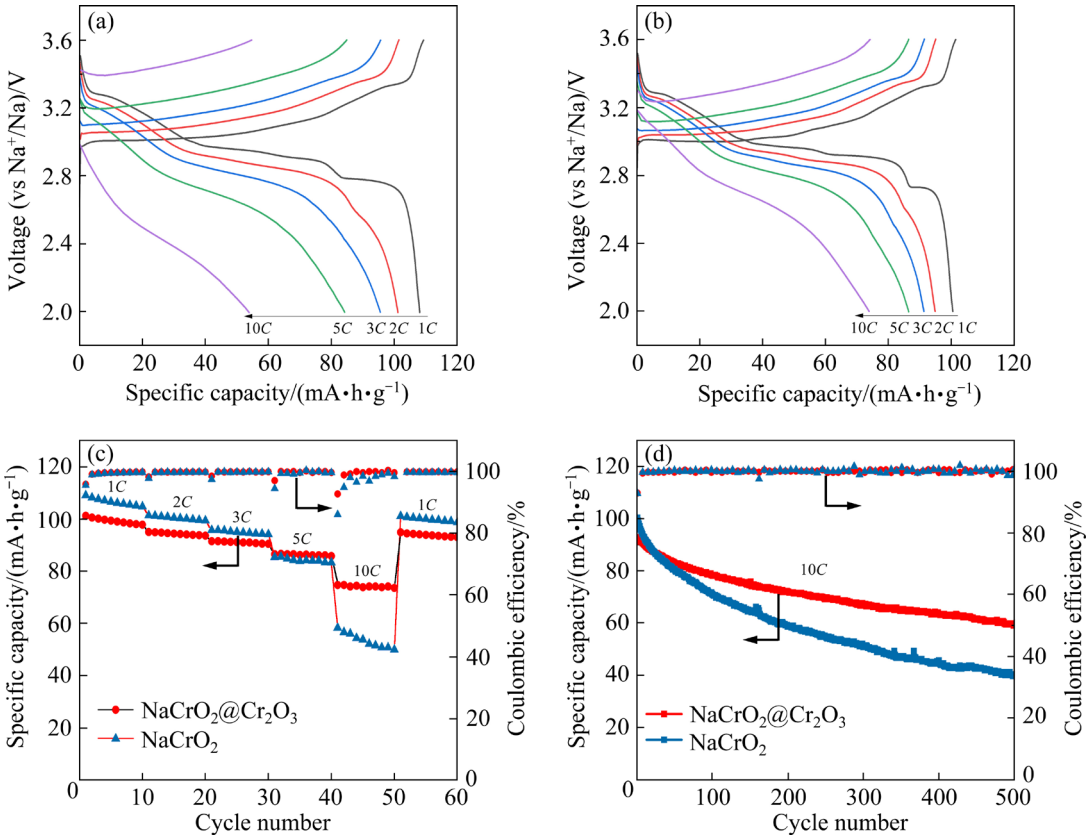


**Fig. 5** Typical charge/discharge profiles of $NaCrO_2$ (a) and $NaCrO_2$@$Cr_2O_3$ (b) at various rates; Rate behaviors (c) and cycling performance at 10$C$ (d) of $NaCrO_2$ and $NaCrO_2$@$Cr_2O_3$

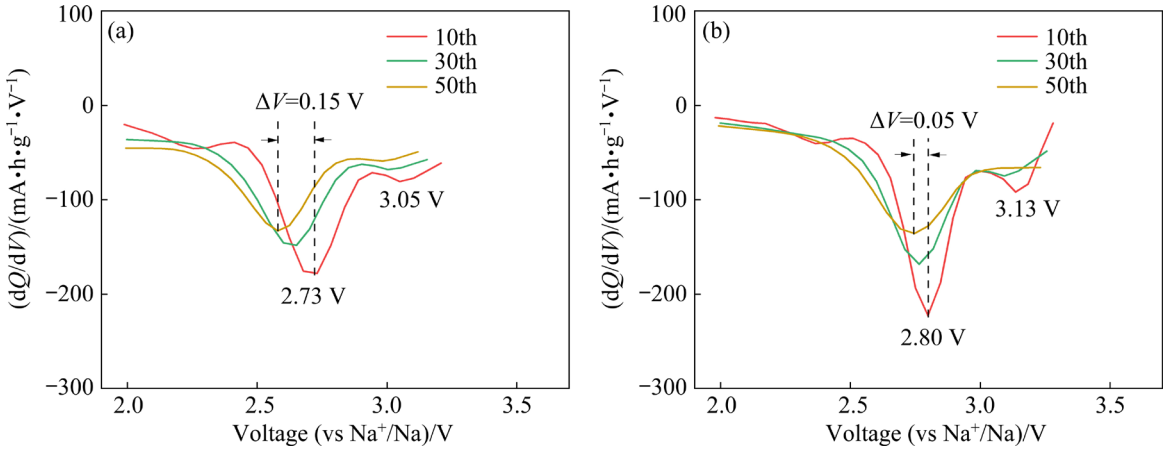


**Fig. 6** d$Q$/d$V$ curves of $NaCrO_2$ (a) and $NaCrO_2$@$Cr_2O_3$ (b) at 10$C$ for different cycles

To further investigate the relationship between the improved electrochemical properties and the surface/interface stability, EIS tests were conducted on the electrodes. Figures 7(a) and 7(b) show the EIS curves of the $NaCrO_2$ and $NaCrO_2$@$Cr_2O_3$ half-cells after 15, 100 and 250 cycles at 10*C*, respectively. All Nyquist plots consist of surface film resistance ($R_f$), charge transfer resistance ($R_{ct}$) and Warburg impedance ($Z_W$), respectively [26,38]. The intercept of the Nyquist plot with the $Z'$-axis represents the ohmic resistance ($R_s$) of $Na^+$ migration in the electrolyte. The EIS curves were fitted by the Z-View software and the fitted data are summarized in Table 2. It can be seen that the $R_{ct}$ values of the $NaCrO_2$@$Cr_2O_3$ after 15, 100 and 250 cycles are 36.8, 68.4 and 72.9 Ω, respectively, and the $R_f$ values of the $NaCrO_2$@$Cr_2O_3$ are 20.5, 33.9 and 48.7 Ω, which are both much less than those of the $NaCrO_2$. This indicates that the $Cr_2O_3$ coating does not cause negative kinetic effects, but rather modifies the interfacial reaction of the material, which is favorable to the $Na^+$ insertion/extraction at high rate.

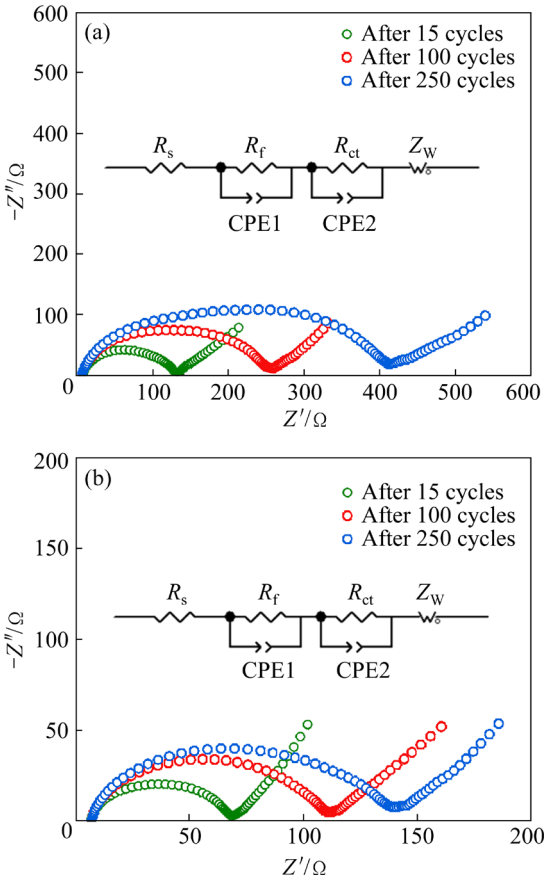


**Fig. 7** Nyquist plots and corresponding equivalent circuit model diagrams of $NaCrO_2$ (a) and $NaCrO_2$@$Cr_2O_3$ (b) electrodes at 10*C* after different cycles

**Table 2** EIS parameters of equivalent circuits of $NaCrO_2$ and $NaCrO_2$@$Cr_2O_3$ electrodes after different cycles

| Sample | Cycle No. | $R_s$/Ω | $R_f$/Ω | $R_{ct}$/Ω |
|---|---|---|---|---|
| $NaCrO_2$ | 15 | 7.8 | 76.2 | 43.8 |
| | 100 | 7.0 | 108.7 | 122.7 |
| | 250 | 6.9 | 126.7 | 266.1 |
| $NaCrO_2$@$Cr_2O_3$ | 15 | 6.7 | 20.5 | 36.8 |
| | 100 | 6.8 | 33.9 | 68.4 |
| | 250 | 6.6 | 48.7 | 72.9 |

## 4 Conclusions

(1) A uniform $Cr_2O_3$ coating layer is in situ constructed on the surface of $NaCrO_2$ by controlling the excess ratio of sodium source. The content of $Cr_2O_3$ in the $NaCrO_2$@$Cr_2O_3$ is 1.73 wt.%, and the coating thickness is about 3 nm. The $Cr_2O_3$-coated sample consists of polygonal-shaped particles with particle size of about 1 μm.

(2) The uniform $Cr_2O_3$ coating on the surface improves the surface/interface stability and reduces the polarization of $NaCrO_2$, which greatly improves the electrochemical performance of $NaCrO_2$.

(3) The $Cr_2O_3$ coating layer prevents the direct contact between the active material and the electrolyte, effectively suppressing the side reactions. The $NaCrO_2$@$Cr_2O_3$ material exhibits enhanced cycling performance, with a capacity retention of 66.4% after 500 cycles at 10*C*.

### CRediT authorship contribution statement

**Mu-lan QIN:** Conceptualization, Formal analysis, Writing − Original draft, Writing − Review & editing, Funding acquisition, Supervision; **Chao HU:** Methodology, Investigation, Data curation, Software, Visualization; **Guo-zhao FANG:** Validation, Resources, Supervision; **Shu-quan LIANG:** Project administration; Resources; **Wan-min LIU:** Software, Supervision; **Bin SHEN**: Software, Visualization.

### Declaration of competing interest

The authors declare that they have no known competing financial interests or personal relationships that could have appeared to influence the work reported in this paper.

### Acknowledgments

This work was supported by the Scientific Research Fund of Hunan Provincial Education Department, China (No. 22B0741).

## References


[1] ARMAND M, TARASCON J M. Building better batteries [J]. Nature, 2008, 451: 652−657.

[2] GOODENOUGH J B, KIM Y. Challenges for rechargeable Li batteries [J]. Chemistry of Materials, 2010, 22: 587−603.

[3] CHENG Fang-yi, LIANG Jing, TAO Zhan-liang, CHEN Jun. Functional materials for rechargeable batteries [J]. Advanced Materials, 2011, 23: 1695−1715.

[4] PAN Hui-lin, HU Yong-sheng, CHEN Li-quan. Room-temperature stationary sodium-ion batteries for large-scale electric energy storage [J]. Energy & Environmental Science, 2013, 6: 2338−2360.

[5] RONG Xiao-hui, LU Ya-xiang, QI Xing-guo, ZHOU Quan, KONG Wei-he, TANG Kun, CHEN Li-quan, HU Yong-sheng. Na-ion batteries: From fundamental research to engineering exploration [J]. Energy Storage Science and Technology, 2020, 9: 515−522.

[6] LV Wei-jun, HUANG Zhi-gao, YIN Ya-xia, YAO Hu-rong, ZHU Hai-liang, GUO Yu-guo. Strategies to build high-rate cathode materials for Na-ion batteries [J]. ChemNanoMat, 2019, 5: 1253−1262.

[7] LIANG Shu-quan, GUO Shao, HE Wei, CAO Xin-xin, MA Jun-jian, ZHOU Jiang, FANG Guo-zhao. New exploration based on crystal chemistry of ion migration and energy storage mechanism in anion-close-packed cathode materials for rechargerable battery [J]. The Chinese Journal of Nonferrous Metals, 2024, 34(6): 1769−1785. (in Chinese)

[8] LV Wei-jun, GAN Lu, YUAN Xin-guang, ZHENG Yong-ping, HUANG Yi-yin, ZHENG Li-tuo, YAO Hu-rong. Understanding the aging mechanism of Na-based layered oxide cathodes with different stacking structures [J]. ACS Applied Materials & Interfaces, 2022, 14: 33410−33418.

[9] YAO Hu-rong, ZHENG Li-tuo, XIN Sen, GUO Yu-guo. Air-stability of sodium-based layered-oxide cathode materials [J]. Science China Chemistry, 2022, 65: 1076−1087.

[10] QIN Mu-lan, YIN Chang-yu, XU Wen, LIU Yang, WEN Jun-hao, SHEN Bin, WANG Wei-gang, LIU Wan-min. Facile synthesis of high capacity P2-type $Na_{2/3}Fe_{1/2}Mn_{1/2}O_2$ cathode material for sodium-ion batteries [J]. Transactions of Nonferrous Metals Society of China, 2021, 31: 2074−2080.

[11] LIANG Yong, WU Hu, LIU Wan-min, QIN Mu-lan, TANG Ze-xun, SHEN Bin, WANG Wei-gang, LIU Qiang. Effect of the calcination temperature on the morphology, structure and electrochemical properties of $Na_{0.67}Ni_{0.11}Cu_{0.11}Fe_{0.3}Mn_{0.48}O_2$ nanoparticles as cathode material for Na batteries [J]. ACS Applied Nano Materials, 2024, 7: 17768−17775.

[12] KOMABA S, TAKEI C, NAKAYAMA T, OGATA A, YABUUCHI N. Electrochemical intercalation activity of layered $NaCrO_2$ vs $LiCrO_2$ [J]. Electrochemistry Communications, 2010, 12: 355−358.

[13] YABUUCHI N, IKEUCHI I, KUBOTA K, KOMABA S. Thermal stability of $Na_xCrO_2$ for rechargeable sodium batteries: Studies by high-temperature synchrotron X-ray diffraction [J]. ACS Applied Materials and Interfaces, 2016, 8: 32292−32299.

[14] XIA X, DAHN J R. $NaCrO_2$ is a fundamentally safe positive electrode material for sodium-ion batteries with liquid electrolytes [J]. Electrochemical and Solid-State Letters, 2012, 15: 2−6.

[15] ZHOU Yong-ning, DING Jing-jing, NAM K W, YU Xi-qian, BAK S M, HU En-yuan, LIU Jue, BAI Jian-ming, LI Hong, FU Zheng-wen, YANG Xiao-qing. Phase transition behavior of $NaCrO_2$ during sodium extraction studied by synchrotron-based X-ray diffraction and absorption spectroscopy [J]. Journal of Materials Chemistry A, 2013, 1: 11130−11134.

[16] KUBOTA K, IKEUCHI I, NAKAYAMA T, TAKEI C, YABUUCHI N, SHIIBA H, NAKAYAMA M, KOMABA S. New insight into structural evolution in layered $NaCrO_2$ during electrochemical sodium extraction [J]. Journal of Physical Chemistry C, 2015, 119: 166−175.

[17] BO Shou-huang, LI Xin, TOUMAR A J, CEDER G. Layered-to-rock-salt transformation in desodiated $Na_xCrO_2$ ($x$=0.4) [J]. Chemistry of Materials, 2016, 28: 1419−1429.

[18] DING Jing-jing, ZHOU Yong-ning, SUN Qian, FU Zheng-wen. Cycle performance improvement of $NaCrO_2$ cathode by carbon coating for sodium ion batteries [J]. Electrochemistry Communications, 2012, 22: 85−88.

[19] BHARDWAJ A, PANWAR A K. Effect of carbon shell over $NaCrO_2$ core by $C_2H_2$ decomposition to enhance electrochemical properties for rechargeable sodium-ion batteries [J]. Applied Surface Science, 2022, 573: 151449.

[20] WU Jia-hui, HU Guo-rong, DU Ke, PENG Zhong-dong, HUANG Min, FAN Ju, GONG Yi-fan, GUAN Di-chang, SHI You, LIU Rui-rui, CAO Yan-bing. Inhibiting electrochemical phase transition of $NaCrO_2$ with long-cycle stability by surface fluorination treatment [J]. Electrochimica Acta, 2022, 403: 139641.

[21] LI Wei, WANG Yong, HU Guo-rong, PENG Zhong-dong, CAO Yan-bing, ZENG Yue-xi, DU Ke. Ti-doped $NaCrO_2$ as cathode materials for sodium-ion batteries with excellent long cycle life [J]. Journal of Alloys and Compounds, 2019, 779: 147−155.

[22] WANG Yue-sheng, CUI Pei-xin, ZHU Wen, FENG Zi-min, VIGEANT M J, DEMERS H, GUERFI A, ZAGHIB K. Enhancing the electrochemical performance of an O3-$NaCrO_2$ cathode in sodium-ion batteries by cation substitution [J]. Journal of Power Sources, 2019, 435: 226760−226767.

[23] XI Kai-ying, CHU Shu-fen, ZHANG Xiao-yu, ZHANG Xue-ping, ZHANG Hao-yang, XU Hang, BIAN Jing-jing, FANG Tian-cheng, GUO Shao-hua, LIU Pan, CHEN Ming-wei, ZHOU Hao-shen. A high-performance layered Cr-based cathode for sodium-ion batteries [J]. Nano Energy, 2020, 67: 104215−104221.

[24] LEE I, OH G, LEE S, YU T Y, ALFARUQI M H, MATHEW V, SAMBANDAM B, SUN Y K, HWANG J Y, KIM J. Cationic and transition metal co-substitution strategy of O3-type $NaCrO_2$ cathode for high-energy sodium-ion batteries [J]. Energy Storage Materials, 2021, 41: 183−195.

[25] MA Cui, LI Xun-lu, YUE Xin-yang, BAO Jian, LUO Rui-jie, ZHOU Yong-ning. Suppressing O3-O'3 phase transition in $NaCrO_2$ cathode enabling high rate capability for sodium-ion batteries by Sb substitution [J]. Chemical Engineering Journal, 2022, 432: 134305.

[26] WANG Yong, LI Wei, HU Guo-rong, PENG Zhong-dong, CAO Yan-bing, GAO Hong-cai, DU Ke, GOODENOUGH J B. Electrochemical performance of large-grained $NaCrO_2$ cathode materials for Na-ion batteries synthesized by decomposition of $Na_2Cr_2O_7{\cdot}2H_2O$ [J]. Chemistry of Materials, 2019, 31: 5214−5223.

[27] LIANG Long-wei, SUN Xuan, DENIS D K, ZHANG

Jin-yang, HOU Lin-rui, LIU Yang, YUAN Chang-zhou. Ultralong layered $NaCrO_2$ nanowires: A competitive wide-temperature-operating cathode for extraordinary high-rate sodium-ion batteries [J]. ACS Applied Materials & Interfaces, 2019, 11: 4037−4046.

[28] WANG Shuo, CHEN Fei, HE Xiao-dong, ZHANG Li-ming, CHEN Fang, WANG Jun-ru, DONG Jie-min, CHEN Chun-hua. Self-template synthesis of $NaCrO_2$ sub-microspheres for stable sodium storage [J]. ACS Applied Materials & Interfaces, 2021, 13: 12203−12210.

[29] YU C Y, PARK J S, JUNG H G, CHUNG K Y, AURBACH D, SUN Y K, MYUNG S T. $NaCrO_2$ cathode for high-rate sodium-ion batteries [J]. Energy & Environmental Science, 2015, 8: 2019−2026.

[30] KALIYAPPAN K, LIU Jian, XIAO Bi-wei, LUSHINGTON A, Li Ru-ying, SHAM T K, SUN Xue-liang. Enhanced performance of P2-$Na_{0.66}(Mn_{0.54}Co_{0.13}Ni_{0.13})O_2$ cathode for sodium-ion batteries by ultrathin metal oxide coatings via atomic layer deposition [J]. Advanced Functional Materials, 2017, 27: 1701870−1701877.

[31] YU Yang, KONG Wei-jin, LI Qing-yuan, NING De, SCHUMACHER Ge, SU Chun-jian, LIU Xiang-feng. Understanding the multiple effects of $TiO_2$ coating on $NaMn_{0.33}Fe_{0.33}Ni_{0.33}O_2$ cathode material for Na-ion batteries [J]. ACS Applied Energy Materials, 2020, 3: 933−942.

[32] CHANG Yi-jiao, XIE Guang-hui, ZHOU Yong-mao, WANG Jie-xi, WANG Zhi-xing, GUO Hua-jun, YOU Bian-zheng, YAN Guo-chun. Enhancing storage performance of P2-type $Na_{2/3}Fe_{1/2}Mn_{1/2}O_2$ cathode materials by $Al_2O_3$ coating [J]. Transactions of Nonferrous Metals Society of China, 2022, 32: 262−272.

[33] ŞAHAN H, GÖKTEPE H, PATAT Ş, ÜLGEN A. Effect of the $Cr_2O_3$ coating on electrochemical properties of spinel $LiMn_2O_4$ as a cathode material for lithium battery applications [J]. Solid State Ionics, 2010, 181: 1437−1444.

[34] CHENG Cui-xia, YI Hui-yang, CHEN Fang. Effect of $Cr_2O_3$ coating on $LiNi_{1/3}Co_{1/3}Mn_{1/3}O_2$ as cathode for lithium-ion batteries [J]. Journal of Electronic Materials, 2014, 43: 3681−3687.

[35] ZOU Hai-lin, LIANG Xin, WANG Zhong-hui, CHENG Sheng, XIANG Hong-fa. Preparation of $Li_4Ti_5O_{12}$ microspheres with a pure $Cr_2O_3$ coating layer and its effect for lithium storage [J]. Chinese Journal of Chemical Physics, 2017, 30: 103−111.

[36] WANG Shuo, CHEN Fei, ZHU Tian-yuan, HE Xiao-dong, LIAO Jia-ying, ZHANG Li-ming, DING Xiang, HU Qiao, CHEN Chun-hua. In situ-formed $Cr_2O_3$ coating on $NaCrO_2$ with improved sodium storage performance [J]. ACS Applied Materials & Interfaces, 2020, 12: 44671−44678.

[37] IKHE A B, PARK W B, MANASI M, AHN D, SOHN K S, PYO M. Unprecedented cyclability and moisture durability of $NaCrO_2$ sodium-ion battery cathode via simultaneous Al doping and $Cr_2O_3$ coating [J]. ACS Applied Materials & Interfaces, 2023, 15: 14958−14969.

[38] MATHIYALAGAN K, PONNAIAH A, KARUPPIAH K, RENGAPILLAI S, MARIMUTHU S. Enhanced performance on layered O3-$Na_{0.95}CrO_2$ cathode material for emerging sodium-ion batteries [J]. Ionics, 2020, 26: 3929−3936.

[39] CHEN C Y, MATSUMOTO K, NOHIRA T, HAGIWARA R, FUKUNAGA A, SAKAI S, NITTA S, INAZAWA S. Electrochemical and structural investigation of $NaCrO_2$ as a positive electrode for sodium secondary battery using inorganic ionic liquid NaFSA-KFSA [J]. Journal of Power Sources, 2013, 237: 52−57.

[40] MENG Xiang-cong, LIANG Jin-ji, LIANG Min, LI Wen-ya, LIN Chen-han, KE Xi, SHI Zhi-cong, LIU Li-ying. Superior rate performance and structural evolution of O3-type layered $NaCrO_2$ for sodium ion batteries at high temperatures [J]. Science China Materials, 2023, 66: 3445−3452.

[41] BAEK M, KIM J, JEONG K, YANG S, KIM H, LEE J, KIM M, KIM K J, CHOI J K. Naked metallic skin for homo-epitaxial deposition in lithium metal batteries [J]. Nature Communications, 2023, 14: 1296.

[42] LIANG Jin-ji, LIU Li-ying, LIU Xiang-si, MENG Xiang-cong, ZENG Lin-yong, LIU Jun, LI Jie, SHI Zhi-cong, YANG Yong. O3-type $NaCrO_2$ as a superior cathode material for sodium/potassium-ion batteries ensured by high structural reversibility [J]. ACS Applied Materials Interfaces, 2021, 13: 22635−22645.

# 钠离子电池 $NaCrO_2$@$Cr_2O_3$ 正极材料的构建与电化学性能

秦牡兰[1]，胡 超[2]，方国赵[2]，梁叔全[2]，刘万民[1]，申 斌[1]

1. 湖南工程学院 材料与化工学院，湘潭 411104；
2. 中南大学 材料科学与工程学院，长沙 410083

**摘 要：**层状 O3 型 $NaCrO_2$ 正极材料在储钠过程中与电解液的副反应严重影响了其电化学性能。通过控制钠源过量比，在 $NaCrO_2$ 正极材料表面原位构建一层均匀的 $Cr_2O_3$ 包覆层，并对包覆材料的结构、形貌、价态和电化学性能进行表征。结果表明，$Cr_2O_3$ 包覆层不会改变 $NaCrO_2$ 的晶体结构和形貌，但能有效抑制 $NaCrO_2$ 与电解液之间的副反应，提高 $NaCrO_2$ 材料的表/界面稳定性。$Cr_2O_3$ 包覆 $NaCrO_2$ 正极材料显示出更好的电化学性能，以 10*C* 循环 500 次后容量保持率达到 66.4%。

**关键词：**$NaCrO_2$；$Cr_2O_3$；钠离子电池；正极材料；电化学性能

**(Edited by Bing YANG)**